PNAS RESEARCH ARTICLE | CHEMISTRY

Biolistic delivery of liposomes protected in metal-organic frameworks

Sneha Kumari[a], Yalini H. Wijesundara[a], Thomas S. Howlett[a], Mohammad Waliullah[b], Fabian C. Herbert[a], Arun Raja[a], Ikeda Trashi[a], Rodrigo A. Bernal[b], and Jeremiah J. Gassensmith[a,c,1]

Edited by Chad Mirkin, Northwestern University, Evanston, IL; received October 29, 2022; accepted February 3, 2023

Needle-and-syringe-based delivery has been the commercial standard for vaccine administration to date. With worsening medical personnel availability, increasing biohazard waste production, and the possibility of cross-contamination, we explore the possibility of biolistic delivery as an alternate skin-based delivery route. Delicate formulations like liposomes are inherently unsuitable for this delivery model as they are fragile biomaterials incapable of withstanding shear stress and are exceedingly difficult to formulate as a lyophilized powder for room temperature storage. Here we have developed a approach to deliver liposomes into the skin biolistically—by encapsulating them in a nano-sized shell made of Zeolitic Imidazolate Framework-8 (ZIF-8). When encapsulated within a crystalline and rigid coating, the liposomes are not only protected from thermal stress, but also shear stress. This protection from stressors is crucial, especially for formulations with cargo encapsulated inside the lumen of the liposomes. Moreover, the coating provides the liposomes with a solid exterior that allows the particles to penetrate the skin effectively. In this work, we explored the mechanical protection ZIF-8 provides to liposomes as a preliminary investigation for using biolistic delivery as an alternative to syringe-and-needle–based delivery of vaccines. We demonstrated that liposomes with a variety of surface charges could be coated with ZIF-8 using the right conditions, and this coating can be just as easily removed—without causing any damage to the protected material. The protective coating prevented the liposomes from leaking cargo and helped in their effective penetration when delivered into the agarose tissue model and porcine skin tissue.

biolistic delivery | biomimetic mineralization | shear stress | zeolitic imidazolate frameworks | metal-organic frameworks

Significance

Syringe-based delivery of vaccines has several drawbacks that call for the investigation of effective alternatives for skin route-based delivery. Biolistic delivery is a promising alternative, but the high shear stress and the requirement that liposomes be formulated as dry powders make such an approach impossible due to the biomaterial's fragility. Here, we demonstrate a cost-effective, needle-free method of delivering cargo-loaded liposomes into the skin via biolistic delivery. This study leads us in a promising direction of future research where the clinical relevance of biolistic delivery could be further investigated without much concern for damage caused to the encapsulated biomaterials in the process.

Biomaterials for healthcare applications have seen a paradigm shift over the last few decades. Targeting specific pathways to mitigate illness while minimizing side effects has prompted research to move toward developing more sophisticated delivery systems. Viral vectors for gene therapy (1) and drug-loaded mesoporous silica (2) are a few examples of compound therapeutics and prophylactics used in medicine today. Among these delivery systems, lipid-based platforms have stolen the limelight in the last few years, as lipid nanoparticle messenger ribonucleic acid (mRNA) vaccines mRNA-1273 (Moderna) and BNT162b2 (BioNTech) hit the clinic to curb the spread of Covid-19. Liposomes are another example of lipid-based delivery vehicles often used to deliver immunostimulatory agents into the body (3, 4), and are used in commercially available vaccines like Cervavix, Epaxal, and Shingrix (5).

Lipid-based nanocarriers are not without issues, however. They are not stable for prolonged periods at room temperature and are susceptible to aggregation, leaky packing, or lipid fusion into multilamellar structures (6). They are shipped and stored within an expensive logistical network called "the cold chain", which helps maintain strict environmental controls on the medication—some even requiring −80 °C freezers for the duration of their trip from manufacturer to clinic. The cold chain not only significantly increases the cost of vaccines but is also a problematic barrier to accessibility in places with limited or fluctuating power supply. Developing a method to ship these vaccines without refrigeration can help combat the problem. One promising approach is coating easily degradable biomacromolecules in metal-organic frameworks (MOF). MOFs are coordination polymers that are stable at higher temperatures and have been reported to stabilize biomaterials in their matrix while preserving the integrity of the biological system. Zeolitic Imidazolate Frameworks (ZIF) are amongst the most well-studied MOFs for their potential in medicinal applications. They have bio-friendly synthetic conditions and have been reported to successfully encapsulate a wide array of biomaterials—ranging from small molecule drugs (7, 8), to nucleic acids (9, 10), and microorganisms (11, 12). They can be stored in a dry powder-like form, and the crystals can

Author affiliations: [a]Department of Chemistry and Biochemistry, University of Texas at Dallas, Richardson, TX 75080-3021; [b]Department of Mechanical Engineering, University of Texas at Dallas, Richardson, TX 75080-3021; and [c]Department of Biomedical Engineering, University of Texas at Dallas, Richardson, TX 75080-3021

Author contributions: S.K., Y.H.W., R.A.B., and J.J.G. designed research; S.K., Y.H.W., T.S.H., M.W., F.C.H., A.R., I.T., and R.A.B. performed research; S.K., M.W., and R.A.B. analyzed data; and S.K. and J.J.G. wrote the paper.

The authors declare no competing interest.

This article is a PNAS Direct Submission.

[1]To whom correspondence may be addressed. Email: gassensmith@utdallas.edu.

This article contains supporting information online at https://www.pnas.org/lookup/suppl/doi:10.1073/pnas.2218247120/-/DCSupplemental.

Published March 6, 2023.

protect the encapsulated material against heat and other stress factors faced during long-distance transportation (13).

Another issue brought to the forefront in the last few years is the low healthcare personnel per capita numbers in highly populated areas of the world. Most vaccinations today are delivered via syringe and needle, requiring technical skills that cannot be transferred to the general population or volunteers quickly. Disposable needles result in biohazardous waste, and their accidental (or intentional) reuse spreads blood-borne pathogens worldwide. While intramuscular injections are more straightforward than intravenous injections, they are prone to neurovascular injuries. On the other hand, subcutaneous injections can result in the permeation of formulations parallel to the subcutaneous region instead of perpendicular, depending on the speed of administration (14). This can result in the formation of misshapen depots of drug or vaccine in the layers of skin, resulting in a different release pattern than anticipated. The general aversion to needles—especially in children—may deter vaccinating via both these administration routes. Attempting to mitigate these challenges makes investigating alternate vaccine administration methods an enticing research prospect.

Biolistic delivery is an alternative route of vaccine administration worthy of exploration, as its entry path is through the skin, mimicking a needle-syringe-based route. This technique involves firing microprojectiles into a target using controlled mechanical force via a ballistic particle delivery system. Once optimized, biolistic delivery systems can deliver materials with the same speed and pressure in every repetition, offering an advantage over injection-based systems where the speed and accuracy rely on the medical professional. While the traditional use of biolistic delivery was aimed at plants for gene transfection (15–17), in the last couple of decades, several groups have shown that materials delivered biolistically can penetrate the epidermis and lodge themselves in the dermis region effectively (18, 19). Gold or tungsten microparticles are commonly used for cargo loading in commercially available gene guns. The materials are loaded on the outside and hence exposed to shearing forces from the pressure of the gun. Lipid-based formulations tend to leak under shear stress, as previously demonstrated (20) by Natsume and Yoshimoto—a finding we confirm in our investigation below. Without any protective outer coating, liposomes cannot be delivered via gene guns. Traditional gene guns also have the added financial burden of requiring a continuous supply of gold for preparing "bullets", which are both unsuitable for lipid-based formulations and very expensive to implement on a large scale.

Considering the above factors, we have developed (21) an inexpensive biolistic delivery system called a "MOF-Jet" to deliver materials in solid powder and liquid suspension form. Although versatile, this system was initially designed to provide sensitive materials encapsulated in MOFs. In this work, we demonstrate that we can exploit biolistic routes of administration to deliver liposomal platforms in ZIF-8 irrespective of surface charge, where ZIF-8 provides biomaterial protection against shear forces and adequate mechanical strength to penetrate through the skin (Fig. 1). We hypothesized that liposomes might be challenging to deliver through the skin biolistically due to their bubble-like construction. Their poor resistance against vibration (22), shear stress, and lack of rigidity might cause the liposomes to leak or not penetrate the surface effectively. Liposomes of various surface charges were successfully protected in ZIF-8 for biolistic delivery and showed that neither the processes of ZIF-8 encapsulation nor the biolistic delivery disrupts the liposome's size or lamellarity. Furthermore, we show that the ZIF-8 shells provide the liposomes with adequate rigidity to penetrate the tissue model and a significant population of the particles lodge themselves in the dermis level.

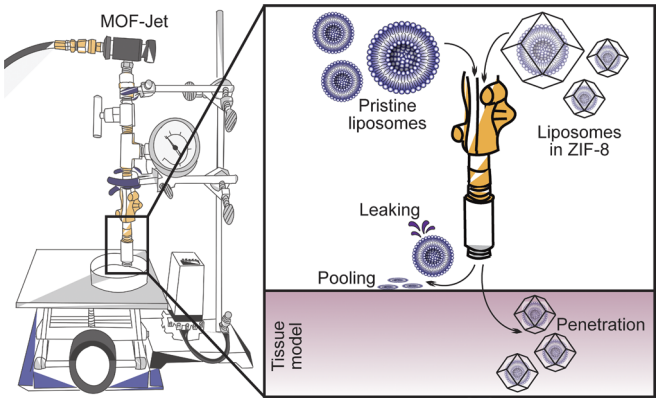

Fig. 1. Comparative studies between pristine and ZIF-8-coated liposomes demonstrate the mechanical stability of the ZIF-8 coating. Pristine liposomes leak under the shear stress of the MOF-Jet, while ZIF-8-coated liposomes remain protected and negligible leaking is observed. The hard coating of the ZIF-8 allows the coated liposomes to penetrate into the tissue model, while the pristine liposomes just pool on the surface.

Results and Discussion

To develop a protection mechanism that could be applied to various lipid-based vaccines, we aimed to test the consistency of ZIF-8 coatings on different types of liposomes. A library of liposomes demonstrating a variety of surfaces was synthesized using a mixture of charged, uncharged, and polyethylene glycol-conjugated lipids and were correspondingly named cationic (Cat), neutral (Neu), anionic (Ani), and PEGylated (PEG). The liposomes were characterized using Transmission Electron Microscopy (TEM) (Fig. 2 *A–D*) and Dynamic Light Scattering (DLS) (Fig. 6 *F–I* "pristine") to confirm their ~200 nm size range and unilamellar nature. ζ-potential (Fig. 2*G*) of all liposomes was measured to ensure that varying the lipid compositions afforded us the variety in surface charge, which would help us test ZIF-8 crystal growth on different nucleating surfaces. Dye-encapsulated versions of all four liposomes using the fluorescent dye Cyanine 5 (Cy5) were also synthesized

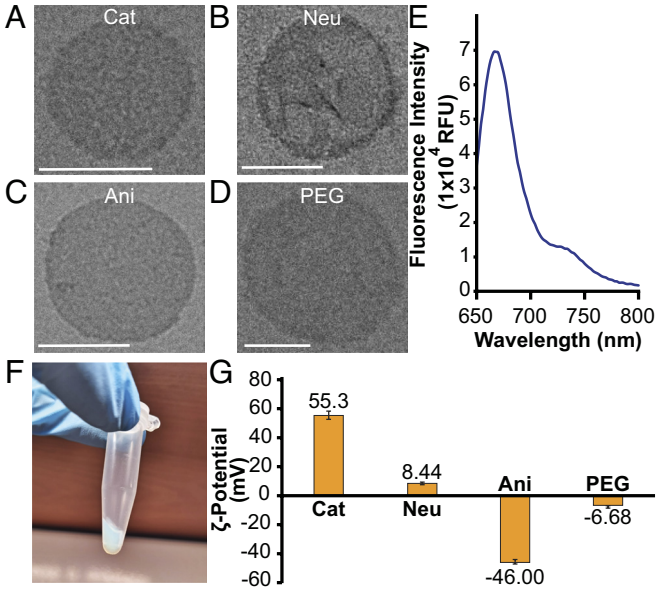

Fig. 2. (*A–D*) TEM micrographs of pristine Cat, Neu, Ani, and PEG liposomes. (Scale bar, 200 nm for all micrographs.) (*E*) Fluorescence spectrum of Cy5@Neu. (*F*) Pellet of Cy5@Neu obtained after ultracentrifugation at 160,000× g and removal of excess Cy5 dye in the supernatant. No significant differences were observed between the fluorescence spectra and pellets of Cy5@Neu, Cy5@Cat, Cy5@Ani, and Cy5@PEG. (*G*) ζ-potential of pristine Cat, Neu, Ani, and PEG liposomes.

(named Cy5@Cat/Neu/Ani/PEG), whose fluorescence spectra (Fig. 2*E*) were recorded as well. Since Cy5@Lip was prepared by adding Cy5 to the buffer in which the liposomes were prepared, the excess unencapsulated dye was subsequently removed from the supernatant post ultracentrifugation at 160,000× g to obtain a light blue pellet (Fig. 2*F*).

To demonstrate the versatility of ZIF-8 encapsulation, all four liposomes were encapsulated in ZIF-8 using four different ligand/metal (L/M) molar ratios that were varied in the synthetic conditions for encapsulation. The zinc acetate precursor's final concentration was kept fixed at 20 mM, while the L/M ratios tested were 4, 8, 16, and 32. Each of these conditions was tested for a reaction time of 3 h and 24 h. The choice of optimal conditions aimed to maximize the liposomes' encapsulation efficiency (Fig. 3 *A*–*D*) while minimizing adhesion of unencapsulated liposomes to free ZIF-8 (*SI Appendix*, Fig. S1). At higher L/M ratios of 16 and 32—especially in a 24-h setup—we observe excellent encapsulation efficiencies regardless of the surface charge. We selected these two L/M ratios for further investigation and characterized them using powder X-ray diffraction (PXRD) (Fig. 3*E*) and scanning electron microscopy (SEM) (Fig. 3*F*). The PXRD of all liposomes encapsulated in L/M 16 and 32 indicate sodalite crystal structure of the products. While literature suggests (23) that biomimetic mineralization is most successful when the nucleating surface has an anionic charge, our fine-tuned conditions allow the encapsulation of neutral and even cationic liposomes. It is clear from watching the reaction proceed that the liposomes themselves induce nucleation of the crystalline ZIF-8. As shown in the supplemental recording (Movie S1) of the reaction, which captures the first 5 min of the reaction, it is clear that there is a rapid formation of a white flocculate shortly after addition of the ZIF-8 precursors. In contrast, when ZIF-8 precursors are added to water, no crystallization is observed at all, suggesting the reaction is facilitated by the liposomes themselves. To understand the kinetics of the biomimetic mineralization process better, we checked the encapsulation efficiency of Cy5@Neu in ZIF-8 (L/M ratio 32) at various time points between 15 min and 3 h and observed that the encapsulation efficiency was already 77.8% at the 15 min mark (*SI Appendix*, Fig. S2). When Cy5@Lip was encapsulated inside ZIF-8, the composite exhibited fluorescence as visualized by epifluorescence microscopy (Fig. 3*G*).

Our investigation aimed to determine whether the ZIF-8 coating is necessary and beneficial in protecting the liposomes from shear stress damage. To test that, we compared the biolistic delivery of pristine and encapsulated liposomes delivered through the MOF-Jet (*SI Appendix*, Fig. S3). Initial attempts to biolistically deliver pristine liposomes into a vial showed no significant change in size upon applying mechanical pressure when measured through DLS (*SI Appendix*, Fig. S4). Next, we tested how the shear stress would affect leaking of components encapsulated inside the liposome (dye, in our case). A common approach in drug and vaccine development research is to encapsulate small-molecule drugs or adjuvants inside the lumen of the liposomes; preventing leaking in such cases is crucial to delivering the expected dose. We used a cone-and-plate viscometer at four different shear rates to quantify the shear stress applied. As the shear stress was increased on the viscometer, we observed higher leaking of the encapsulated dye. This was done by encapsulating 5,6-carboxyfluorescein (CF)—a self-quenching dye—inside the liposome and quantifying the leaking using fluorescence intensities (*SI Appendix*, Fig. S5). The dye inside the liposomes is quenched owing to its high concentration, and as CF leaks out, it regains fluorescence. We observed that the relationship between shear stress and leaking was linear; thus, we used these measurements as a standard to quantify the shear stress applied by the MOF-Jet at various pressures on the delivered material (*SI Appendix*, Table S1). We replicated the experiment performed using the viscometer, but this time using the MOF-Jet. We not only observed the linear relationship between shear stress and leaking again, but also found that almost 35% of the encapsulated dye leaked at 4,137 kPa. We encapsulated CF@Lip in ZIF-8 using L/M 16 and 32 and compared their leaking at different pressures with that of unprotected CF@Lip. Both of the ZIF-8-encapsulated formulations showed negligible leaking, indicating that the coating was very effective in preventing escape of the encapsulated cargo

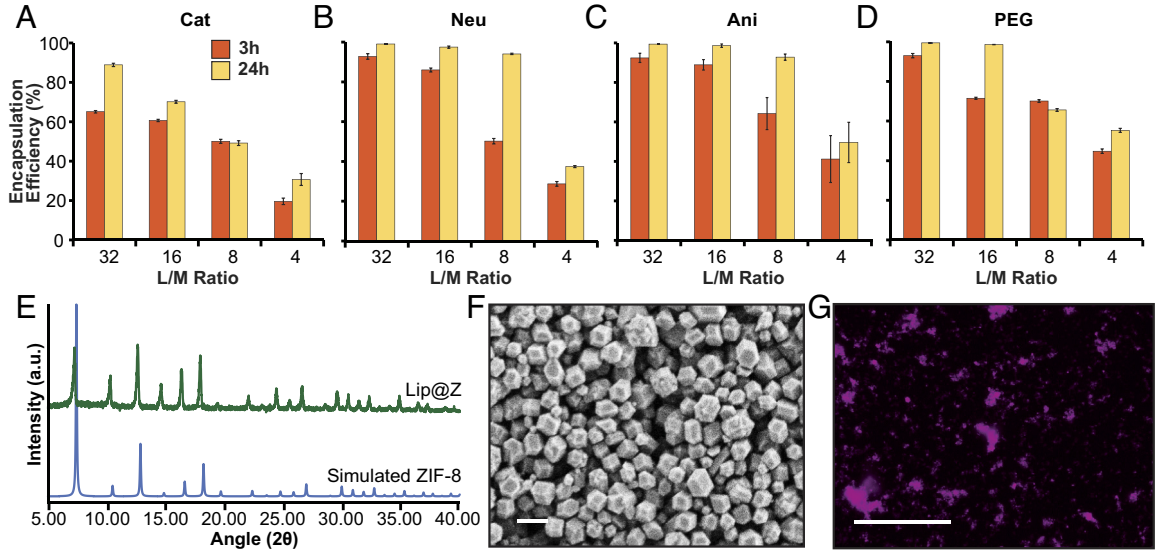

Fig. 3. (*A*–*D*) Encapsulation efficiencies of Cy5@Cat, Cy5@Neu, Cy5@Ani, and Cy5@PEG liposomes at various L/M ratios. Each of the liposomes was encapsulated in ZIF-8 by adding ZnOAc and HMIM such that the L/M ratios were 32, 16, 8, and 4—as labeled on the *x* axis. All conditions were measured for encapsulation efficiencies after 3 h (orange) and 24 h (yellow). Measurements were performed by quantifying the percentage of unencapsulated Cy5@Lip in the supernatant using fluorescence. Error bars are represented as ±SD. (*E*) PXRD pattern of Neu@Z-32 and simulated ZIF-8. (*F*) SEM micrograph of Neu@Z-32. (Scale bar, 1 μm.) (*G*) Epifluorescence micrograph of Neu@Z-32. (Scale bar, 100 μm.) No significant differences were observed in the PXRD patterns, SEM micrographs, and epifluorescence micrographs of Neu@Z-32, Cat@Z-32, Ani@Z-32, PEG@Z-32, Neu@Z-16, Cat@Z-16, Ani@Z-16, and PEG@Z-16.

(*SI Appendix*, Fig. S6). As a control experiment, we incubated CF@Lip in 20 mM zinc acetate, 2-methylimidazole, and water as a baseline to check whether these reagents individually caused the liposomes to leak (*SI Appendix*, Fig. S7). While 2-methylimidazole did not affect the liposomes, we found that zinc could disrupt the lipid bilayer as some leaking of CF into the solution was evident, especially after 1 h. It is worth noting that this leakage is likely not significant during the reaction given the fast rate of the reaction discussed above. Further, 2-methylimidazole is added in 32:1 stoichiometric excess compared to zinc, which would favor an early interaction between zinc and 2-methylimidazole rather than the zinc and phosphates from the phospholipids. Further work on the mechanism of this reaction is ongoing.

It is worth noting that prevention of cargo leaking is not the only function the ZIF-8 coating serves when used as a protective coating for biolistic delivery. The ZIF-8 crystals provide the desired structural rigidity—absent in pristine liposomes—required for effective penetration of the particles into the tissue. Atomic force microscopy (AFM) combined with nanoindentation has been previously employed to determine the mechanical properties of MOFs and liposomes individually (24–27). We use this technique to record and compare the fracture force of Lip@Z against literature reports of unencapsulated, unilamellar ~200 nm liposomes and quantify the additional rigidity provided to our system. We measured the compressive force individual particles withstand under the indentation of the AFM tip (Fig. 4*A*). We conducted indentations on Neu@Z-32 and on ~250 nm ZIF-8 crystals as a control. In most cases, the fracture caused by the tip is clearly visible under the microscope (Fig. 4*B*). The force-displacement curves show an increase in force as the particle is indented, followed by particle fracture (Fig. 4*C*). We tabulate fracture force as the largest peak in force measured in the curve (Fig. 4*D*). ZIF-8 particles have a slightly higher fracture force when compared to Lip@Z, but they are all within the same μN range of force. Most noteworthy, Lip@Z and control ZIF-8 particles are significantly stronger than bare ~200 nm liposomes, whose fracture force is reported in the order of 100pN-1nN (28). It is worth noting that fracture force has an element of size dependence, and the difference between ZIF-8 and Lip@Z may be partially attributed to the small difference in size.

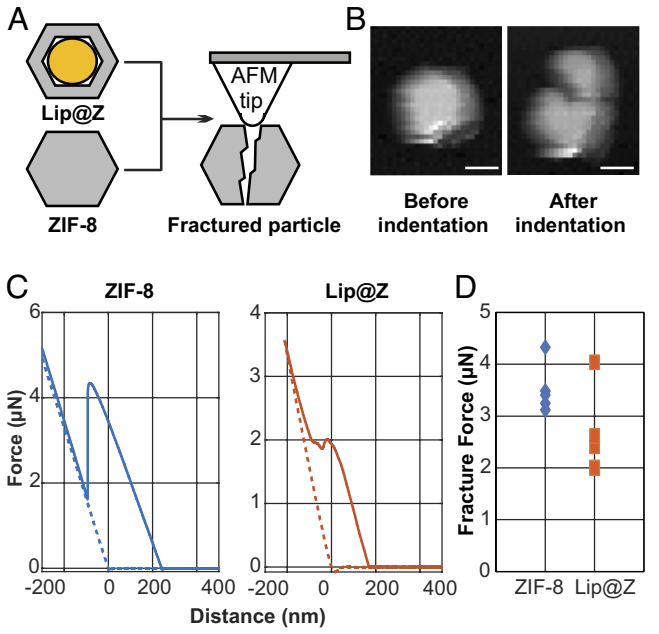

Fig. 4. (*A*) Schematic illustration of AFM nano-indentation of ZIF-8 and Lip@Z crystals. (*B*) Image of Lip@Z crystal captured before and after nano-indentation. (Scale bar, 100 nm for both images.) (*C*) Single representative force-displacement curves of free ZIF-8 control and Lip@Z, respectively. (*D*) Fracture force of ZIF-8 and Lip@Z measured from the force-displacement curves (n = 5 for each).

To test how this mechanical strength translates into our desired application of biolistic skin-based delivery, we performed preliminary experiments to qualitatively assess the difference between the penetration profiles of Cy5@Lip and Cy5@Lip@Z. Upon delivering unencapsulated Cy5@Lip into a 2% agarose tissue model using the MOF-Jet, the liposome suspension simply pooled on the agarose gel surface without any significant penetration (*SI Appendix*, Fig. S8). When repeated with Cy5@Lip@Z, particles embedded inside the gel were visible when cross-sectioned and imaged under the epifluorescence microscope (*SI Appendix*, Fig. S9). While this assessment indicates that particles penetrate well with the help of the ZIF-8 coating, it is crucial to know how the payload would distribute across

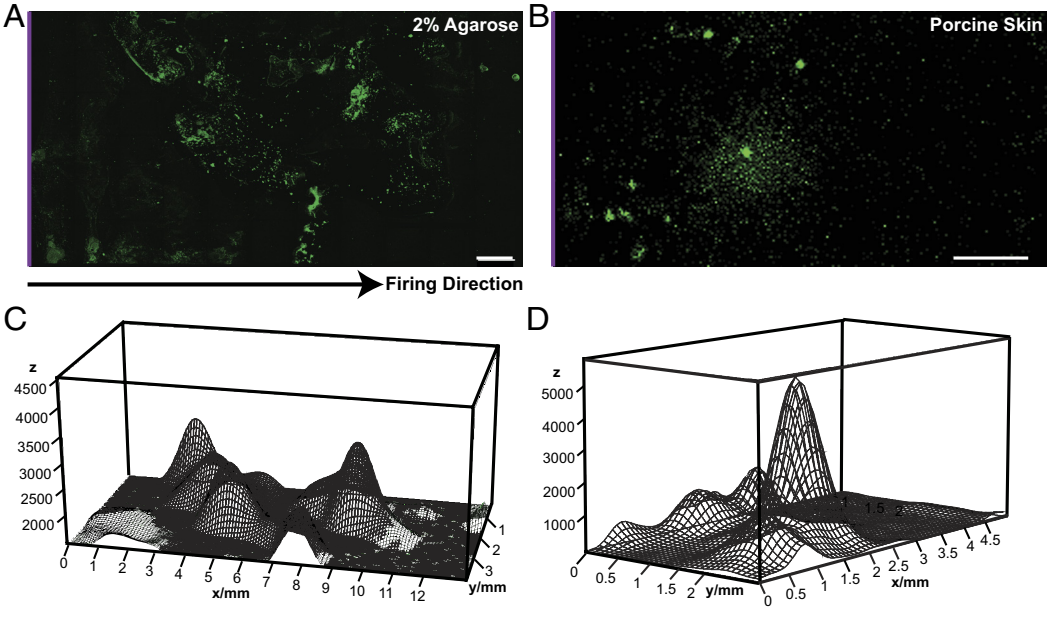

Fig. 5. (*A* and *B*) Maximum intensity projection of the confocal Z-stack image of Cy5@Neu@Z-32 delivered biolistically into agarose tissue model and porcine skin tissue. Cy5@Neu@Z-32 was first delivered into a 2% agarose gel tissue model at 2,068 kPa with a nozzle-to-gel distance of 2 cm, and into porcine skin tissue at 4,826 kPa with a nozzle-to-tissue distance of 0.5 cm. The sample was then flipped onto a clean surface to avoid dragging the particles deeper into the gel, and cross-sectioned using a sharp blade. The cross-sectioned specimen was placed on a #0 coverslip with the top surface (depth = 0 mm, marked with a purple line) on the reader's left, and confocal micrographs were captured. (Scale bar, 1 mm.) (*C* and *D*) three-dimensional population density plot representing the distribution of Cy5@Neu@Z-32 within the gel and tissue calculated from the overlay image shown in Fig. 3 *A* and *B*, respectively. The plots were generated using Fiji (image processing and analysis software).

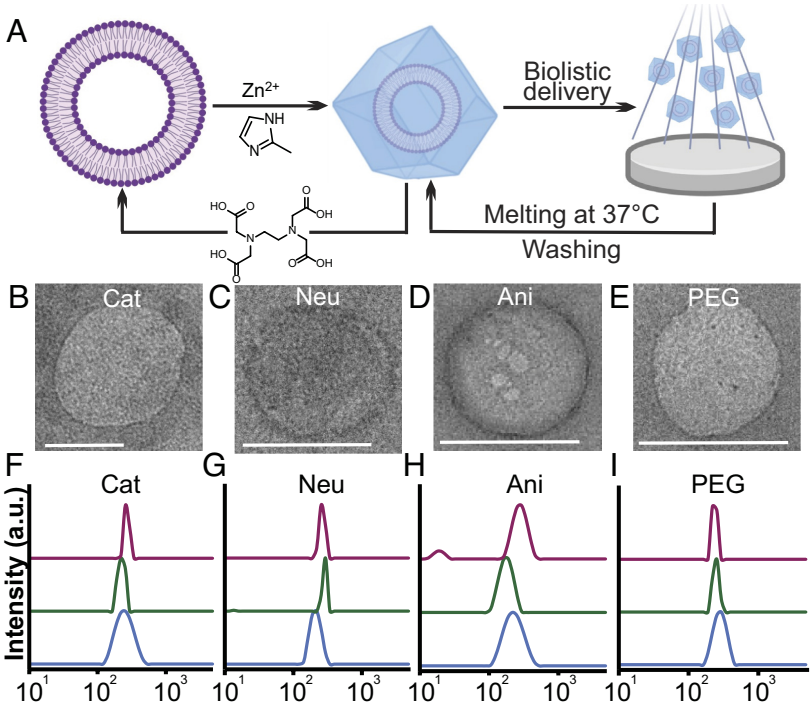

Fig. 6. (*A*) Experimental scheme illustrating the steps of the recovery experiment—i) encapsulation of liposomes in ZIF-8, ii) biolistic delivery of Lip@Z using MOF-Jet into 5% gelatin A ballistic gel at 2,068 kPa with a nozzle-to-gel distance of 2 cm, iii) removal of gelatin by melting, centrifuging at 37 °C, washing twice, and iv) chemical exfoliation of ZIF-8 coating using 0.5M EDTA as a chelating agent at 4 °C left overnight on a rotisserie. (*B–E*) TEM micrographs of Cat, Neu, Ani, and PEG liposomes after the recovery experiment were performed using Cat@Z-32, Neu@Z-32, Ani@Z-32, and PEG@Z-32, respectively. (Scale bar, 200 nm for all micrographs.) No significant differences were observed in the TEM micrographs when the recovery experiment was performed using Cat@Z-16, Neu@Z-16, Ani@Z-16, and PEG@Z-16. (*F–I*) DLS graphs of Cat, Neu, Ani, and PEG liposomes in pristine form (blue), after recovery from Lip@Z-16 (green) and Lip@Z-32 (magenta). Lip represents Cat/Neu/Ani/PEG in each respective graph. The X-axis of all graphs represents liposome size in nm.

the epidermis and dermis when delivered into the skin. We repeated the biolistic delivery of Cy5@Lip@Z on the agarose tissue model (Fig. 5*A*) and on porcine skin tissue (Fig. 5*B*), but this time imaged the cross-sections and obtained a Z-stack on a confocal microscope. Even though 2% agarose is a known and published tissue model mimicking (29) the density of soft tissue, its elasticity and toughness are poorly represented by the gel. There is a noticeable difference in penetration depth of both when compared side by side. The fluorescence of the Cy5@Lip@Z population was integrated at each depth to obtain a density plot for both samples to help the readers better visualize the particle distribution within the agarose or porcine tissue post-biolistic delivery (Fig. 5 *C* and *D*).

There is extensive research on the use of ZIF coatings for biomaterials used in drug and vaccine delivery models since the kinetic lability of the ZIF coatings make it easy to remove in the presence of a chelating agent, acidic pH, or a phosphate-rich environment. As ZIF-8 is known to degrade in tissues over several days to 2 wk, there is promising application scope for this technique in pharmaceutics. To confirm that the process of encapsulation and removal of the ZIF-8 coating does not damage the liposomes, we chemically "exfoliate" the ZIF-8 coating from all the Lip@Z variants using EDTA as a chelating agent. The recovered liposomes were characterized using TEM and were all observed to be a similar size as observed prior to encapsulation (*SI Appendix*, Fig. S10). When a ZIF-8-protected vaccine is to be delivered biolistically in a clinical setting, other stress factors are also at play. To simulate such a series of events, we i) encapsulated our liposomes in ZIF-8, ii) biolistically delivered them into 5% type A gelatin ballistic gel, iii) melted the gel at physiological temperatures, and iv) exfoliated the ZIF-8 coating using EDTA to recover the liposomes back (Fig. 6*A*). The choice of 5% gelatin A was based on its low melting temperature and its ability to withstand 2,068 kPa pressure on the MOF-Jet. The recovered liposomes were characterized for their lamellarity and size range using TEM (Fig. 6 *B–E*) and DLS (Fig. 6 *F–I*). We were satisfied to observe that the liposomes remain unilamellar, and their final size was close to that of the pristine formulations. There were some very low-intensity peaks under 50 nm observed at times with the DLS, but we suspect them to be small aggregates of salts and gelatin still remaining in solution. This once again demonstrates the outstanding preservation of delicate biomaterials that the exterior ZIF-8 coating can provide—robust enough to even deliver through a pressurized biolistic delivery system.

Conclusion

In this work, we explored the mechanical protection ZIF-8 provides to liposomes as a preliminary investigation for using biolistic delivery as an alternative to syringe-and-needle-based delivery of vaccines. We demonstrated that a wide variety of surfaces of delicate biomaterials could be coated using ZIF-8 using the right conditions, and this coating can be just as easily removed—without causing any damage to the protected material. The protective coating prevented the liposomes from leaking cargo and helped in effective penetration of the sample when delivered into the tissue model and porcine skin tissue. Together, all these conclusions lead us in a very promising direction of future research where the clinical relevance of biolistic delivery could be further investigated without much concern for damage caused to the biomaterials in the process.

Materials and Methods

Chemicals. 18:0 PC (DSPC) 1,2-distearoyl-sn-glycero-3-phosphocholine, 18:1 TAP (DOTAP) 1,2-dioleoyl-3-trimethylammonium-propane (chloride salt), 18:1 (Δ9-Cis) PE (DOPE) 1,2-dioleoyl-sn-glycero-3-phosphoethanolamine, 18:1 PA

(DOPA) 1,2-dioleoyl-sn-glycero-3-phosphate (sodium salt) and 18:0 PEG2000 PE 1,2-distearoyl-sn-glycero-3-phosphoethanolamine-N- [methoxy (polyethylene glycol)-2000] (ammonium salt) were purchased from Avanti Polar Lipids. MOPS 3-(4-morpholino) propane sulfonic acid, TCEP tris(2-carboxyethyl) phosphine, sodium chloride, and chloroform were purchased from Fisher Scientific. Synthesis and characterization of cyanine-5-carboxylic acid used has been reported by Luzuriaga et al. (11) Zinc acetate dihydrate, 2-methylimidazole, sodium hydroxide, 5(6)-carboxyfluorescin and gelatin type A (from porcine skin) were purchased from Millipore Sigma. Porcine tissue was purchased from Sierra for Medical Science. Ethylenediaminetetraacetic acid was purchased from Cole-Parmer. Agarose (molecular biology grade) was purchased from Research Products International.

Instruments. Liposomes were extruded using Avanti Mini Extruder. Cy5@Lip was pelleted down using Sorvall MX-120 micro-ultracentrifuge. Fluorescence spectra of Cy5@Lip were recorded using Horiba Fluorolog fluorimeter. DLS measurements for size and zeta potential of liposomes were carried out using Malvern Analytical Zetasizer Nano ZS. TEM micrographs of pristine, exfoliated, and recovered liposomes were taken on Japan Electron Optics Laboratory 1400 transmission electron microscope. Fluorescence intensity measurements for calculation of encapsulation efficiency, surface attachment and leaking of liposomes were carried out using Biotek Synergy H4 Hybrid microplate reader. SEM micrographs of Lip@Z were taken using Zeiss Supra 40. PXRD spectra were determined using Rigaku SmartLab X-ray diffractometer. Shear stress was applied on the CF@Lip using Anton Paar Modular Compact Rheometer 302. AFM nanoindentation was carried out on Asylum MFP-3D AFM. Epifluorescence images of Cy5@Lip in agarose, Cy5@Lip@Z both in solution and in agarose were taken on EVOS FL digital inverted fluorescence microscope. Z-stack penetration depth images were taken on Olympus FV3000 RS confocal microscope.

Synthesis of Liposomes. Liposomes were synthesized by first preparing a thin film of 37.5 mg DSPC with 12.5 mg of DOTAP for cationic, DOPE for neutral, DOPA for anionic, and PEG-2000-PE for PEGylated. The lipids were dissolved in 2 mL chloroform and dried out in vacuum conditions. The lipid thin film was then resuspended in 2 mL M-buffer (100mM NaCl, 1mM TCEP, 20mM MOPS) and freeze-thawed 4 to 5 times (30). In the case of Cy5-encapsulated liposomes, the resuspension M-buffer also included 0.05 mg/mL Cy5-Carboxylate. In CF-encapsulated liposomes, the resuspension M-buffer had 7.525 mg/mL 5,6-carboxyfluorescein, and 4M NaOH was added dropwise to the resuspension M-buffer till the dye completely dissolved. The liposomes were then extruded serially through 1 μm, 400 nm, and 200 nm membrane filters to obtain monodispersed liposomal suspensions of around ~200 nm size. For the Cy5-encapsulated liposomes, the excess Cy5 in the supernatant was eliminated by two rounds of ultracentrifugation at 160,000× g, 4 °C, 45 min, following which the supernatant was exchanged with fresh M-buffer each time.

Encapsulation in ZIF-8. Each of the liposome combinations was encapsulated in four different formulations of ZIF-8. The final concentration of reagents in each encapsulation is described in Table 1. After adding reagents, the formulations were incubated for 24 h and then washed twice. For washing, the formulations were centrifuged at 4,000× g for 15 min at RT, and the supernatant was exchanged with deionized (DI) water. After washing, Lip@Z was dried under vacuum conditions overnight to obtain a crystalline solid. Encapsulation of Cy5@Lip followed the same procedure.

Leaking Studies and Estimation of Shear Stress from MOF-Jet. Two hundred microliters of CF@Lip suspension was loaded onto the bullet of the MOF-Jet and delivered at 1,379 kPa (200 PSI) into an empty scintillation vial. The process was repeated with 2,758 kPa (400 PSI) and 4,137 kPa (600 PSI). Each biolistically delivered sample was diluted 20× and measured for its fluorescence intensity against pristine CF@Lip of the same batch diluted 20×. To quantify the shear stress from the MOF-Jet, 200 μL of CF@Lip was sheared on a cone-and-plate viscometer at 350/s, 700/s, 1,050/s, and 1,400/s, respectively, for 60 s at 25 °C. All the samples were collected after shearing, diluted 20×, and their fluorescence intensity was quantified for leaked dye.

Table 1. Synthesis conditions for Lip@Z

Lip@Z Formulation	Ligand/Metal ratio	Concentration of ZnOAc (mM)	Concentration of Lipids (mg/mL)	Concentration of 2-Methylimidazole (mM)
Z-4	4	20	0.2	80
Z-8	8	20	0.2	160
Z-16	16	20	0.2	320
Z-32	32	20	0.2	640

Estimation of Encapsulated and Surface-Attached Liposomes. The first supernatant obtained upon centrifugation after ZIF-8 encapsulation was measured for its fluorescence intensity to calculate the encapsulation efficiency of the liposomes in ZIF-8. This was compared to the fluorescence intensity at the start to compare and estimate the percentage of liposomes that remained unencapsulated and were left behind in the supernatant. After two rounds of washing with DI water and drying the Lip@Z samples under vacuum overnight, they were resuspended in methanol to dissolve the surface-attached liposomes. The supernatant obtained upon centrifugation was measured for its fluorescence intensity. This was compared to the fluorescence intensity obtained by drying the same volume of liposome suspension added to the reaction mixture under vacuum and resuspending in methanol to compare and estimate the percentage of liposomes that electrostatically attached themselves to the ZIF-8 crystals and could not be removed by washing with water.

Estimation of Fracture Force by AFM Nanoindentation. The measurement was conducted using a silicon cantilever of constant 17 N/m, calibrated with the Sader method (31). The particles were deposited over a silicon substrate. A tapping mode scan was performed to image the surface and identify the target particle, followed by indentation up to fracture, and a subsequent image was taken to see the changes.

Preparation of Ballistic Gels. For agarose gels, 2% agarose solution was heated and then cast in a cylindrical mould (diameter = 1 in, height = 0.5 in) and cooled at room temperature till solidified. 5% gelatin A solution was heated and cast in the same mold for gelatin gels. Both gels were stored in a closed container at 4 °C for future use.

Penetration Depth Study. For the tissue model, 3 mg of Cy5@Lip@Z was loaded onto the bullet of the MOF-Jet and delivered into 2% agarose gel at 2,068 kPa (300 PSI) and nozzle distance of 2 cm from the top gel surface. For porcine tissue, 3 mg of Cy5@Lip@Z was loaded onto the bullet of the MOF-Jet and delivered into porcine tissue 4,826 kPa (700 PSI) and nozzle distance of 0.5 cm from the top tissue surface. Each respective sample was flipped upside down and longitudinally sectioned to avoid dragging particles along the blade. The section was laid flat on a #0 coverslip for confocal microscope imaging.

Exfoliation and Recovery from Ballistic Gel. For the control exfoliation, Lip@Z obtained from 1 mL reaction volume was exfoliated using 2 mL of 0.25 M EDTA at 4 °C for 18 h on a rotisserie. For the recovery experiment, Lip@Z was loaded onto the bullet of the MOF-Jet and delivered into 5% gelatin A gel at 2,068 kPa (300 PSI) and nozzle distance of 2 cm from the top gel surface. The gel was then cut into 2 to 3 pieces and carefully transferred to a 15-mL centrifuge tube. The samples were centrifuged for 15 min at 4,000× g at 37 °C, and the supernatant was exchanged with DI water. This washing process was repeated twice to ensure minimal gelatin remained in the vial. The extracted Lip@Z was exfoliated using the procedure above.

Data, Materials, and Software Availability. All study data are included in the article and/or *SI Appendix*. Raw data is available in Open Science Framework (https://osf.io/2jge4/?view_only=a2711d05023d4ece9b1a4fc0d68d341a) (32).

ACKNOWLEDGMENTS. S.K. acknowledges Diana Alatalo for her guidance in using the rheometer and Ved Prakash for his help in obtaining the confocal Z-stack images. J.J.G. acknowledges the NSF [Grant no. DMR-2003534] and the Welch Foundation [Grant no. AT-1989-20190330] for their support and funding.

1. Z. Zhao, A. C. Anselmo, S. Mitragotri, Viral vector-based gene therapies in the clinic. *Bioeng. Transl. Med.* **7**, e10258–e10258 (2021).
2. T. I. Janjua, Y. Cao, C. Yu, A. Popat, Clinical translation of silica nanoparticles. *Nat. Rev. Mater.* **6**, 1072–1074 (2021).
3. R. Tenchov, R. Bird, A. E. Curtze, Q. Zhou, Lipid nanoparticles—from liposomes to mRNA vaccine delivery, a landscape of research diversity and advancement. *ACS Nano* **15**, 16982–17015 (2021).
4. J. Zhuang *et al.*, Nanoparticle delivery of immunostimulatory agents for cancer immunotherapy. *Theranostics* **9**, 7826–7848 (2019).
5. D. Chatzikleanthous, D. T. O'Hagan, R. Adamo, Lipid-based nanoparticles for delivery of vaccine adjuvants and antigens: Toward multicomponent vaccines. *Mol. Pharm.* **18**, 2867–2888 (2021).
6. P. Kour, G. Rath, G. Sharma, A. K. Goyal, Recent advancement in nanocarriers for oral vaccination. *Artif. Cells Nanomed. Biotechnol.* **46**, S1102–S1114 (2018).
7. I. B. Vasconcelos *et al.*, Cytotoxicity and slow release of the anti-cancer drug doxorubicin from ZIF-8. *RSC Adv.* **2**, 9437–9442 (2012).
8. C. Wang *et al.*, Metal-organic framework encapsulation preserves the bioactivity of protein therapeutics. *Adv. Healthc. Mater.* **7**, e1800950–e1800950 (2018).
9. O. R. Brohlin *et al.*, Zeolitic imidazolate framework nanoencapsulation of CpG for stabilization and enhancement of immunoadjuvancy. *ACS Appl. Nano Mater.* **5**, 13697–13704 (2022), 10.1021/acsanm.1c03555.
10. A. Poddar *et al.*, ZIF-C for targeted RNA interference and CRISPR/Cas9 based gene editing in prostate cancer. *Chem. Commun.* **56**, 15406–15409 (2020).
11. M. A. Luzuriaga *et al.*, Enhanced stability and controlled delivery of MOF-encapsulated vaccines and their immunogenic response in vivo. *ACS Appl. Mater. Interfaces* **11**, 9740–9746 (2019).
12. M. A. Luzuriaga *et al.*, Metal-organic framework encapsulated whole-cell vaccines enhance humoral immunity against bacterial infection. *ACS Nano* **15**, 17426–17438 (2021).
13. F. C. Herbert *et al.*, Stabilization of supramolecular membrane protein–lipid bilayer assemblies through immobilization in a crystalline exoskeleton. *Nat. Commun.* **12**, 2202 (2021).
14. H. Kim, H. Park, S. J. Lee, Effective method for drug injection into subcutaneous tissue. *Sci. Rep.* **7**, 9613–9613 (2017).
15. T. M. Klein, E. D. Wolf, R. Wu, J. C. Sanford, High-velocity microprojectiles for delivering nucleic acids into living cells. *Nature* **327**, 70–73 (1987).
16. T. M. Klein, R. Arentzen, P. A. Lewis, S. Fitzpatrick-McElligott, Transformation of microbes, plants and animals by particle bombardment. *Bio/Technology* **10**, 286–291 (1992).
17. K. Miller *et al.*, An improved biolistic delivery and analysis method for evaluation of DNA and CRISPR-Cas delivery efficacy in plant tissue. *Sci. Rep.* **11**, 7695 (2021).
18. P. Peking *et al.*, A gene gun-mediated nonviral RNA *trans*-splicing strategy for *Col7a1* repair. *Mol. Ther. Nucleic Acids* **5**, e287 (2016).
19. S.-W. Tsai *et al.*, Myostatin propeptide gene delivery by gene gun ameliorates muscle atrophy in a rat model of botulinum toxin-induced nerve denervation. *Life Sci.* **146**, 15–23 (2016).
20. T. Natsume, M. Yoshimoto, A method to estimate the average shear rate in a bubble column using liposomes. *Ind. Eng. Chem. Res.* **52**, 18498–18502 (2013).
21. Y. H. Wijesundara *et al.*, Carrier gas triggered controlled biolistic delivery of DNA and protein therapeutics from metal–organic frameworks. *Chem. Sci.* **13**, 13803–13814 (2022).
22. D. M. Klein *et al.*, Degradation of lipid based drug delivery formulations during nebulization. *Chem. Phys.* **547**, 111192 (2021).
23. N. K. Maddigan *et al.*, Protein surface functionalisation as a general strategy for facilitating biomimetic mineralisation of ZIF-8. *Chem. Sci.* **9**, 4217–4223 (2018).
24. Z. Zeng, J.-C. Tan, AFM nanoindentation to quantify mechanical properties of nano- and micron-sized crystals of a metal-organic framework material. *ACS Appl. Mater. Interfaces* **9**, 39839–39854 (2017).
25. A. A. Tiba, A. V. Tivanski, L. R. MacGillivray, Size-dependent mechanical properties of a metal-organic framework: Increase in flexibility of ZIF-8 by crystal downsizing. *Nano Lett.* **19**, 6140–6143 (2019).
26. D. Vorselen, M. C. Piontek, W. H. Roos, G. J. L. Wuite, Mechanical characterization of liposomes and extracellular vesicles, a protocol. *Front. Mol. Biosci.* **7**, 139 (2020).
27. D. Mukherjee *et al.*, Differential flexibility leading to crucial microelastic properties of asymmetric lipid vesicles for cellular transfection: A combined spectroscopic and atomic force microscopy studies. *Colloids Surf. B* **196**, 111363 (2020).
28. Z. Dai *et al.*, Chain-length- and saturation-tuned mechanics of fluid nanovesicles direct tumor delivery. *ACS Nano* **13**, 7676–7689 (2019).
29. N. Zilony, A. Tzur-Balter, E. Segal, O. Shefi, Bombarding cancer: Biolistic delivery of therapeutics using Porous si carriers. *Sci. Rep.* **3**, 2499 (2013).
30. S. S. Abeyrathna *et al.*, IroT/MavN is a legionella transmembrane Fe(ii) transporter: Metal selectivity and translocation kinetics revealed by in vitro real-time transport. *Biochemistry* **58**, 4337–4342 (2019).
31. J. E. Sader *et al.*, Spring constant calibration of atomic force microscope cantilevers of arbitrary shape. *Rev. Sci. Instrum.* **83**, 103705 (2012).
32. J. J. Gassensmith, Biolistic delivery of liposomes protected in metal-organic frameworks. Open Science Framework. https://osf.io/2jge4/?view_only=a2711d05023d4ece9b1a4fc0d68d341a. Deposited 22 February 2023.